AFRL-RX-WP-TR-2014-0105

ADAPTIVE, ACTIVE AND MULTIFUNCTIONAL COMPOSITE AND HYBRID MATERIALS PROGRAM: Composite and Hybrid Materials ERA

Marilyn R. Unroe
AFRL/RXCC

APRIL 2014
Final Report

Approved for public release; distribution unlimited.

See additional restrictions described on inside pages

STINFO COPY

AIR FORCE RESEARCH LABORATORY
MATERIALS AND MANUFACTURING DIRECTORATE
WRIGHT-PATTERSON AIR FORCE BASE, OH 45433-7750
AIR FORCE MATERIEL COMMAND
UNITED STATES AIR FORCE

NOTICE AND SIGNATURE PAGE

AFRL-RX-WP-TR-2014-0105 HAS BEEN REVIEWED AND IS APPROVED FOR PUBLICATION IN ACCORDANCE WITH ASSIGNED DISTRIBUTION STATEMENT.

//Signature//

MARILYN R. UNROE, Program Manager
Composites Branch
Structural Materials Division

//Signature//

DONNA L. BALLARD, Section Chief
Composites Branch
Structural Materials Division

//Signature//

ROBERT T. MARSHALL, Deputy Chief
Structural Materials Division
Materials and Manufacturing Directorate

REPORT DOCUMENTATION PAGE

Form Approved
OMB No. 0704-0188

1. REPORT DATE *(DD-MM-YY)*
April 2014

2. REPORT TYPE
Final

3. DATES COVERED *(From - To)*
01 October 2008 – 30 September 2012

4. TITLE AND SUBTITLE
ADAPTIVE, ACTIVE AND MULTIFUNCTIONAL COMPOSITE AND HYBRID MATERIALS PROGRAM: Composite and Hybrid Materials ERA

5a. CONTRACT NUMBER
In-house

5b. GRANT NUMBER

5c. PROGRAM ELEMENT NUMBER
62102F

6. AUTHOR(S)
Marilyn Unroe

5d. PROJECT NUMBER
4347

5e. TASK NUMBER

5f. WORK UNIT NUMBER
X0BP/BC101100

7. PERFORMING ORGANIZATION NAME(S) AND ADDRESS(ES)
AFRL/RXCC
2941 Hobson Way
Wright-Patterson AFB, OH 45433-7817

8. PERFORMING ORGANIZATION REPORT NUMBER

9. SPONSORING/MONITORING AGENCY NAME(S) AND ADDRESS(ES)
Air Force Research Laboratory
Materials and Manufacturing Directorate
Wright-Patterson Air Force Base, OH 45433-7750
Air Force Materiel Command
United States Air Force

10. SPONSORING/MONITORING AGENCY ACRONYM(S)
AFRL/RXCC

11. SPONSORING/MONITORING AGENCY REPORT NUMBER(S)
AFRL-RX-WP-TR-2014-0105

12. DISTRIBUTION/AVAILABILITY STATEMENT
Approved for public release; distribution unlimited.

13. SUPPLEMENTARY NOTES
PA Case Number: 88ABW-2014-2223; Clearance Date: 12 May 2014. Report contains color.

14. ABSTRACT (*Maximum 200 words*)
This report documents the final summation of a four-year in-house technical program on comprehensive materials development for organic, polymeric and carbonaceous composite and hybrid materials with combined structural loadbearing and other physical properties. The first three years of the four-year effort were comprised of tasks that were exclusively directed to fabrication, characterization and testing of multifunctional composite and hybrid materials for adaptive and shape-memory applications, and carbon fiber materials characterization and development. In the fourth and final year as the Composite and Hybrid Materials Exploratory Research Area (ERA), this bridge program incorporated portions of other areas such as thermal protective systems in extreme environments.

15. SUBJECT TERMS
Ceramic Matrix Composites (CMCs), Polymeric Matrix Composites (PMCs), preceramic, thermal protective system, miscibility, extreme environments, composite materials, hybrid materials, carbon-carbon, carbon fiber

16. SECURITY CLASSIFICATION OF: a. REPORT	b. ABSTRACT	c. THIS PAGE	17. LIMITATION OF ABSTRACT:	18. NUMBER OF PAGES	19a. NAME OF RESPONSIBLE PERSON (Monitor) / 19b. TELEPHONE NUMBER *(Include Area Code)*
Unclassified	Unclassified	Unclassified	SAR	43	Marilyn R. Unroe / (937) 255-9071

Standard Form 298 (Rev. 8-98)
Prescribed by ANSI Std. Z39-18

TABLE OF CONTENTS

Section **Page**

LIST OF FIGURES

LIST OF TABLES

PREFACE

This technical report entitled, "Adaptive, Active and Multifunctional Composite and Hybrid Materials Program: Composite and Hybrid Materials ERA," was prepared by the Composite Materials Branch, Structural Materials Division. The work was initiated under Program Element (PE) Number 62102F, BPACs 624347 and 6201SP, AFRL/RX Work Unit Number X0BP (historic AFRL/RX Work Unit Number BC101100), "Composite and Hybrid Materials Exploratory Research Area (ERA)".

The program was administered under the direction of the Materials and Manufacturing Directorate, Air Force Research Laboratory, Air Force Materiel Command, Wright-Patterson AFB, OH, with Dean Foster as the Program Manager for the overarching three-year Adaptive, Active and Multifunctional Composite and Hybrid Materials Program, and Marilyn R. Unroe and Walter A. Juzukonis as Program Managers for the bridge Composite and Hybrid Materials ERA Program. The author of this technical report was Marilyn R. Unroe. This report summarizes publicly releasable program work of PE Number 62102F conducted from 1 October 2008 through 30 September 2012.

1.0 SUMMARY

This report documents the final summation of a four-year in-house technical effort on a comprehensive materials development program for organic, polymeric and carbonaceous composite and hybrid materials with combined structural loadbearing and other physical properties such as electrical and/or thermal conductivity or resistance, elastomeric shape change as imagined in a muscular contraction and relaxation response to external stimuli, or phase change. This program was named "Adaptive, Active and Multifunctional Composite and Hybrid Materials Program (historic Work Unit Number BC101100).

The first three years of the four-year effort were devoted to tasks that were exclusively directed at the fabrication, characterization and testing of multifunctional composite and hybrid materials for adaptive and shape-memory applications. The objective of the Adaptive, Active and Multifunctional Composite and Hybrid Materials Program was to evaluate mechanical, physical and responsive properties as a function of environmental exposure and then actuating some response. Seven major tasks emanated from this program, some of which continued in the follow-on bridge program to which the Work Unit Number was transferred at the end of Government Fiscal Year (GFY) 2011.

In the fourth and final year as the Composite and Hybrid Materials Exploratory Research Area (ERA) (historic Work Unit Number BC101100), this bridge program incorporated tasks of other capabilities such as thermal protective systems in extreme environments, integrated structural and radio frequency properties and carbon fiber materials characterization and development. As mentioned previously, selective tasks, subtasks and projects of the former program were continued to completion within the ERA.

Within the former AFRL/RXBC Composite and Hybrid Materials Branch of the Materials and Manufacturing Directorate, both the earlier and final programs funded mostly onsite or external project technical efforts which supported the major tasks and subtasks of both programs. Remaining funds of the work unit were used toward the purchase of equipment and laboratory supplies that were needed to conduct the in-house or onsite technical support tasks, and a smaller portion of the funding supported in-house Government associate salaries to conduct in-house projects or support program management activities.

2.0 INTRODUCTION

The historic objective of the Adaptive, Active and Multifunctional Composite and Hybrid Materials Program (AAM) (DTIC Accession #EF005086) was to provide capability of design, modeling, fabrication, processing, and full characterization of novel and developmental polymeric matrix composites (PMCs), hybrid composite materials, and carbonaceous materials with both load-bearing structural and additional physical, mechanical, thermal or electrical properties; hence, the integrated multifunctionality of the resulting materials composition. The approved program was initiated at the start of the Government Fiscal Year GFY 2008 and its four-year term was approved by the AFRL Materials and Manufacturing Directorate (AFRL/RX) Technical Review Board to execute the technical program until GFY 2012 end (Reference 1). At the program start, the work of the program was exclusively directed toward the development of adaptive and active composite and hybrid structural materials that would “adapt” in physical conformation once a stimulus was applied to the target sample structure. Demonstration of this response in a structure was elicited by either a thermal or electrical stimulus, similar in action to the natural response of the conformation of a bird wing during flight vs. takeoff or landing, a muscle pair under flexure or extension, or even the pull-back response of a hand away from a heat source or electrical shock. What was overlooked in this concept until GFY 2009 was the probable requirement that in such an environment, protection from other extraneous stimuli that could cause an undesired, untimely response was needed as well. Therefore, the loadbearing structure would have to move as desired but also possess protection from those extraneous and undesired stimuli, encompassing this idea of multifunctionality for the many real world applications to which this technology could apply.

What seems an unmanageable technical problem to resolve on limited budget and staff was approached by segmentation of the work into palatable tasks and subtasks in a program Work Breakdown Structure (WBS) for the Work Unit designated X0BP. Seven tasks were assigned to the original AAM program WBS with a catch-all task for older work tasks of the branch not quite completed at GFY 2009 start. Due to the drawdown of budgets in GFY 2010 and the consolidation of AFRL/RX organizational structure in GFY 2011, some of the task work mentioned previously continued into GFY 2012 in a one-year bridge program, the Composite and Hybrid Materials Exploratory Research Area (ERA). Uncompleted projects whose terms continued into GFY 2012 were merged into the ERA bridge program: in-house polymer synthesis and processing projects of graded preceramic polymeric hybrid materials, a laser deposition/resin infusion fabrication project, both from the former Hybrid Materials for Extreme Environments Initiative Program (HEE) (DTIC Accession #EF015582) (Reference 2), some ongoing work on nanomaterials synthesis and nanocomposites, and finally characterization of commercial carbon fiber and nanomodified carbon fibers for a Department of Defense carbon fiber database, all of which originated in the AAM parent program.

The entire WBS of the Work Unit’s two programs is described in Table 1. The work of the original three-year AAM overarching program is described in primary Tasks 1.0-7.0 while the HEE ERA inclusions are listed in primary Tasks 8.0-9.0. A Program Management task was included for salaries and effort related to the technical and administrative management of the WBS.

Table 1. Comprehensive WBS (Program Element 6.2 Funded or Co-funded) of the Adaptive, Active and Multifunctional (AAM) Composite and Hybrid Materials Program: Composite and Hybrid Materials ERA.

Primary Tasks	Subtasks	Projects
1.0 Materials with Embedded Functionality	1.1 Support of VDK4000 Direct Write System to Operational Level 1.2 Fabrication and Characterization of Baseline Multifunctional Films Using Commercial off the Shelf (COTS) Materials	1.1.1 Repair and Component Support 1.2.1 Process Optimization of COTS Conductive Inks and Film Substrates for System Calibration 1.2.2 Characterization of COTS Inks and Substrates
2.0 Responsive and Reconfiguring Materials	2.1 Characterization of Skin Materials 2.2 Characterization of Structural Underlayment 2.3 Lightweight Flow and Sensing Methods 2.4 Modeling of Responsive and Reconfiguring Materials	2.1.1 Baseline Characterization of Thermosetting Elastomeric SMP Materials 2.1.2 Bending Mechanics of Azobenzene LCP Films 2.2.1 Baseline Characterization of High Temperature Thermoplastic SMP Foam Microstructure-Mechanical Stress-Strain Relationships 2.2.2 Microvascular Self-Healing Composites Mechanical Evaluation 2.3.1 Z-Axis CNT Growth Using Chemical Vapor Deposition (CVD) on Conductive Substrates 2.3.2 Z-Axis CNT Growth Using CVD on Nonconductive Substrates and CNT Characterization 2.3.3 Lightweight and Bio-inspired Flow Sensing Systems Characterization 2.4.1 3-D Analytical Tool Development for SMPs 2.4.2 Sensory Materials Characterization 2.4.3 Fabrication and Modeling of Rubber Muscle Actuators 2.4.4 Modeling of Power Response of SMP/SMA Microactuation 2.4.5 Modeling of SMP Alloy Composites
3.0 Higher Temperature Shape Memory Materials	3.1 Thermally Activated SMP Synthesis and Fabrication 3.2 Thermally Activated SMCs	3.1.1 High Temperature Thermosetting BMI-Based, Polyaspartimide Resins 3.1.2 Thermosetting non- BMI SMP Neat Resin Characterization and Assessment 3.2.1 Durability Assessment of Fabric Reinforced SMC Laminates 3.2.2 Other Higher Temperature SMCs and Hybrids
4.0 Support of AFOSR Hybrid Material Flight Structures Multi-University Research Initiative (MURI)	4.1 Fabrication of Composite Flat Panels	4.1.1 Fabrication of Bismaleimide (BMI) Resin Panels 4.1.2 Fabrication of BMI/Graphite Composite Panels with Resin Tougheners and Multi-functional Nanofibers

5.0 Nanomodified Carbon and Fiber Characterization for DoD Database	5.1 Commercial Fiber Modifications 5.2 High Temperature Nanotube Yarns and Composite Characterization	5.1.1 Modified High Modulus C-Fiber 5.1.2 Boron Carbide Fiber
6.0 Polymeric Nanocomposites	6.1 Organic and Inorganic Polymer Nanocomposite Alloys 6.2 Polymeric Nanocomposite Battery Materials	6.1.1 DNA/Graphene Oxide (GO) Synthesis, Processing and Characterization 6.1.2 Gold/Polymer Nanocomposites 6.2.1 GO/Polyethylene Oxide (PEO) Synthesis and Processing
7.0 Ongoing Work from AAM for Completion	7.1. Mechanical Testing of Thermosetting Foams for Airfield Matting 7.2 C-Fiber Synthesis and Characterization 7.3 Morphing Materials 7.4 Miscellaneous Durability Subtasks	
8.0 Graded Polymeric-Preceramic Hybrid Materials	8.1 Synthesis of BMI/Preceramic Polymer Compatibilizers 8.2 Processing of BMI/Preceramic Polymer Blends	
9.0 Hybrid Material Fabrication and Processing	9.1 Traditional Processing 9.2 New Processing Approaches	9.2.1 Processing and Fabrication of Hybrid Metal to Composite Joint
10.0 Program Management		

Other limited distribution subtasks and projects of the Composite and Hybrid Materials ERA that are not listed in Table 1 are omitted for the following reasons: the entire subtask or project work is not in the public domain due to contractual considerations, the data is subject to the Arms Export Control Act (Title 22, USC, Sec 2751, et seq.) or the Export Administration Act of 1979, as amended (Title 50, USC, App 2401, et seq.), non-6.2 Program Element funds are used for the task work, or because of application area of the capability which is not in the public domain.

3.0 METHODS AND PROCEDURES

The detailed experimental procedures for each subtask or project of Table 1 were previously described in the open domain citations listed under each Subtask or Project in the Results and Discussion section of this report.

4.0 RESULTS AND DISCUSSION

4.1 Task 1.0 Materials with Embedded Functionality

This primary task consisted of support to establish an in-house capability in the use of a VDK-4000 Direct Write System purchased earlier than the initiation of this overarching program and was divided into three projects that would, at completion, provide a baselined capability in multifunctional film production for experimental and developmental uses. The term of the entire task was October 2008-September 2011.

4.1.1 Support of VDK-400 Direct Write System to Operational Level

4.1.1.1 Repair and Component Support

The first project of the subtask consisted of training and support to get the entire system components acquired and placed in an acceptable laboratory environmental footprint with support infrastructure and debugging of the equipment. The term of this effort was two years with the VDK-4000 finally operational in 2010. Direct write, or mesoscale maskless material deposition, is a processing method by which 3-dimensional integrated structures are built upon thin film substrates that can be themselves either flat or complex in configuration. Metallic and polymer inks and filled adhesives are applied to build the structure using a no contact atomizer and deposition head and deposition is controlled by a computer driven positioning system. In contrast to other conformal deposition processes (e.g., conformal powder coating or wet film spray using electrical current), this technique can build the structure directly without contact of the printing tool with the substrate. If needed the part can then be laser sintered immediately to form a net shape part with well-defined margins and micron level topographic features or cured in an oven using traditional curing or annealing techniques.

4.1.2 Fabrication and Characterization of Baseline Multifunctional Films Using Commercial Off the Shelf (COTS) Materials

4.1.2.1 Process Optimization of COTS Conductive Inks and Film Substrates for System Calibration

This project work consisted of activities that acquired and fabricated test samples from COTS materials to baseline the VDK-4000 capabilities and to calibrate the equipment performance at that reasonable baseline. Commercially available Kapton film was used to fabricate free-standing, unloaded tensile dogbone substrates. Commercially available conductive silver nanoparticle inks were applied to the Kapton films using the Direct Write System. To construct a non-conductive substrate film with a conductive resistor affixed to it, optimization studies were performed for the fabrication parameters with various atomizer pressures, tip sizes and curing cycles.

Public Domain Publications and Presentations: None

4.1.2.2 Characterization of COTS Inks and Substrates

This final characterization project evaluated the overall quality of the actual specimens made with COTS materials in 4.1.2 or made synthetically into inks. Morphology and dispersion of silver nanoparticles were examined by a number of optical imaging techniques including scanning electron microscopy (SEM), atomic force microscopy (AFM), dynamic light scattering (DLS) and transmission electron microscopy (TEM) to assess microstructure and surface interfaces of the inks and the polymer film substrates. Four-probe measurements were accomplished in order to assess electrical resistivity measured in a processed film. It was concluded that final conductivity values were contingent upon initial vendor nanoparticle size and conformation which affects surface morphological and electrical contiguity.

Public Domain Publications and Presentations:

Z. Bai, G. B. Wilks, G. P. Tandon, B. J. Yocum and R. S. Justice, "Functional Silver Nanoink for Direct Write Applications," Proc. ASME 2012 Conf. Smart Mater., Adapt. Struct. and Intell. Sys. (SMASIS2012), 1 (2012) 11-17. SMASIS2012-7922.

4.2 Task 2.0 Responsive and Reconfiguring Materials

The objective of this primary task was to explore and develop a suite of materials, processing, and characterization technologies which enable the essence of the early program's purpose in adaptive and active materials. Subtasks and projects thereof were assigned that encompassed all of the reasonable materials and processing requirements for development of an integrated biomimetic bird or bat wing: skin materials, structural underlayment (the skeleton and muscles) materials, and embedded sensory and circulatory systems. Damage repair of torn or injured tissue was demonstrated by the use of self-healing polymer technology approaches, but the self-healing project work is not described here. Modeling projects were also included in the overall materials development plan. Technical term of the in-house projects was October 2008-September 2011 with some contractual work extensions to April 2013 in order to complete reporting requirements.

4.2.1 Characterization of Skin Materials

Any material ultimately chosen as a shape memory polymer (SMP) composition candidate for skin has these characteristics: ability to endure large deformation (high strain rate), holding of the high strain rate conformation for a period of time, and recovery to its near original size and shape (shape recovery in reversible strain) when triggered by an appropriate stimulus such as temperature, light or other electromagnetic radiation. Amorphous thermoplastic and thermosetting SMP elastomeric materials fit this niche because the isotropic path dependency of properties in crystalline and semi-crystalline oriented polymers is eliminated in an amorphous system. Skin materials possessing varying backbone and end group chemistries and degrees of thermal stability were purchased COTS or prepared synthetically and then fabricated into characterization specimens as described in the following projects.

4.2.1.1 Baseline Characterization of Thermosetting Elastomeric SMP Materials

This project's purpose was to conduct a comprehensive thermomechanical characterization program for commercially available amorphous, thermosetting SMP film elastomeric materials. Unmodified Veriflex^{TM}, Veriflex-E^{TM}, and Veriflex-E2-100^{TM} were acquired from the commercial supplier in order to use this material as a baseline for other compositions of matter purchased, prepared synthetically, or fabricated in order to verify mechanical and physical properties. A thorough thermal analytical examination by Differential Scanning Calorimetry (DSC), Thermogravimetric Analysis (TGA) and Dynamic Mechanical Analysis (DMA) concluded that a post-cure schedule was required to fully cure the as-received Veriflex^{TM} materials. In addition, the complexity of the heterogeneous strain fields in a post-cured thermosetting elastomeric composition such as Veriflex^{TM} indicated mechanical behavior which was dependent upon thermomechanical cycling conditions. To circumvent some of these mechanical behavior problems, thermomechanical testing on an MTS^{TM} load frame using a Digital Image Correlation (DIC) technique helped to establish a test protocol by which thermosetting elastomer films, either neat as an SMP or reinforced as a shape memory composite (SMC), could be evaluated. In addition, a high temperature round tip nanoindentation technique that was developed with other high temperature thermosetting resins compared the thermomechanical behavior of VeriflexE2-100 at various temperatures with DMA values in the bulk for modulus and Poisson's ratio. Thermomechanical cycling dependent behavior was verified by observation of a large elastic strain deformation when samples preheated to near or above glass transition (T_g) temperatures were indented versus samples analyzed from room temperature to the elevated temperature above the T_g of the thermoplastic. Almost complete shape recovery of 99% was observed when preheated (i.e., the deformation and recovery temperatures were above the T_g), indented samples were cooled to room temperature whereas room temperature samples indented while raised to temps above the T_g showed low recovery ratios of their original shapes. The thermomechanical behavior of Veriflex E2-100 samples exposed to environmental conditioning indicated reduced glass transition temperatures, greater weight losses and higher strain and moduli differences globally when compared to unconditioned SMP samples. Shape recovery ratios were also evaluated using the nanoindentation technique described above with lower recovery rates exhibited by UV conditioned and water immersed samples when compared to unconditioned or oil immersed samples. When recovery temperature is above the T_g, shape recovery remains high, indifferent to SMP exposure conditions.

Public Domain Publications (Peer Reviewed) and Presentations:

A. J. McClung, G. P. Tandon, and J. W. Baur, "Deformation Rate-, Hold Time-, and Cycle-Dependent Shape Memory Performance of Veriflex-E^{TM} Resin," J. Mech. of Time-Depend. Mater., 17 (2013) 39-52.

A. J. McClung, G. P. Tandon, and J. W. Baur, "Strain Rate- and Temperature-Dependent Tensile Properties of an Epoxy-Based, Thermosetting, Shape Memory Polymer (Veriflex-E^{TM})," J. Mech. of Time-Depend. Mater. 16 (2012) 205-221.

A. J. McClung, G. P. Tandon, and J. W. Baur, "Relaxation and Recovery Behavior of an Epoxy Based Shape Memory Polymer Resin," Proc. 2012 SEM Ann. Conf. & Expo. Exper. and Appl. Mech. (2012).

Y. C. Lu, J. T. Fulcher, G. P. Tandon, D. C. Foster, and J. W. Baur, "Microscale Thermomechanical Characterization of Environmentally Conditioned Shape Memory Polymers," Polym. Test. 30 (2011) 563-570.

A. J. McClung, G. P. Tandon, K. E. Goecke, and J. W. Baur, "Non-Contact Technique for Characterizing Full-Field Surface Deformation of Shape Memory Polymers at Elevated and Room Temperatures," Polym. Test. 30 (2011) 140-149.

J. T. Fulcher, H. E. Karaca, G. P. Tandon, D. C. Foster, and Y. C. Lu, “Multiscale Characterization of Water, Oil, and UV-Conditioned Shape-Memory Polymer Under Compression,” Proc. 2011 SEM Ann. Conf. and Expo. Exp. and Appl. Mech. 3 (2011) 97-104.

A. McClung, G. P. Tandon, and J. Baur, “Fatigue Cycling of Shape Memory Polymer Resin,” Proc. 2011 SEM Ann. Conf. and Expo. Exp. and Appl. Mech. 3 (2011) 119-127.

J. T. Fulcher, Y. C. Lu, G. P. Tandon, and D. C. Foster, “Thermomechanical Characterization of Shape Memory Polymers Using High Temperature Nanoindentation,” Polym. Test., 29 (2010) 544-552.

J. T. Fulcher, Y. C. Lu, G. P. Tandon, and D. C. Foster, “Thermomechanical Characterization of Environmentally Conditioned Shape Memory Polymers Using Nanoindentation,” Proc. SPIE 7644, Behavior and Mechanics of Multifunctional Materials and Composites 2010, 76440F.

J. T. Fulcher, Y. C. Lu, G. P. Tandon, and D. C. Foster, “Shape Memory Effects of Environmentally Conditioned Shape Memory Polymers Using Nanoindentation,” Proc. SAMPE 2010.

A. J. W. McClung, G. P. Tandon, D. C. Foster, and J. Baur, “Influence of Post-Cure and Repeated Cycling on the Thermomechanical Characterization of Shape Memory Polymers and Composites,” Proc. SAMPE 2010, 138-152.

A. McClung, G. P. Tandon, K. E. Goecke, and J. Baur, “Non-Contact Technique for Characterizing Full-Field Surface Deformation of Shape Memory Polymers,” Proc. ASME 2010 Conf. Smart Mater., Adapt. Struct. and Intell. Sys. (SMASIS2010), 1 (2010) 79-88. SMASIS2010-3679.

A. McClung, G. P. Tandon, and J. Baur, “The Rate-Dependent Mechanical Behavior of Veriflex-E™ in Tension,” Proc. ASME Conf. Smart Mater., Adapt. Struct. and Intell. Sys. (SMASIS2010), 1 (2010) 69-78. SMASIS2010-3674.

Y. C. Lu, G. P. Tandon, D. C. Jones, and G. A. Schoeppner, “Elastic and Viscoelastic Characterization of Thermally-oxidized Polymer Resin Using Nanoindentation,” J. Mech. Time-Dep. Mater. 13 (2009) 245-260.

4.2.1.2 Bending Mechanics of Azobenzene Liquid Crystalline Polymer (LCP) Films

In this project, shape memory LCP polymers with poly(azobenzene) linkages were prepared, films fabricated, and evaluated for shape memory performance. In contrast to the amorphous thermosetting materials of Paragraph 4.2.1.1, these materials are semi-crystalline and thus glassy in nature and isotropic in themomechanical property expression. Film deformation was induced with short wavelengths of polarized blue-green light rather than with heat as described in Paragraph 4.2.1.1. Because of the chemical conformation of the LCP composition, the film undergoes a physical shape change since the absorption of the specific wavelength of light influences the molecular order and overall geometric stacking of the oriented LCP domains. Experiments were described that correlate the number of crosslinked mesogens in the synthesized LCP film compositions and the magnitude of the induced bending and internal stresses observed, all generated by the specific wavelengths of blue or green light to which the films were exposed. Modeling of the strain and deformation rates as a function of materials composition correlated well with the compositions and any external test constraints such as test fixtures and clamps.

Public Domain Publications (Peer Reviewed) and Presentations:

L. Cheng, Y. Torres, K. M. Lee, A. J. McClung, J. Baur, T. J. White, and W. S. Oates, "Photomechanical Bending Mechanics of Polydomain Azobenzene Liquid Crystalline Polymer Network Films," J. Appl. Phys. 112, 013513 (2012); http://dx.doi.org/10.1063/1.4729771

4.2.2 Characterization of the Structural Underlayment

Another set of materials applicable to responsive and reconfiguring materials development are the multi-purpose materials that simulate the porous tissue underlayment of the subcutaneous tissue layers of skin. Intuitively a synthetic foam material would simulate the subcutaneous layers of living tissue; therefore, the quest to find the commercially available material foam useful for traditional runway matting by empirical methods provides dual-use information for simulating a living tissue baseline. That characterization of thermosetting foam filled composite structural sandwich materials under compressive loads is described in Paragraph 4.8.1.

For this subtask, however, tailored low density, highly compressible foam materials of thermoplastic polymer compositions were examined to mimic the impact resistant underlayment of the skin. In addition to environmental conditioning of thermoplastic foams prior to characterization, some of the desired physical characteristics sought in these foams as either SMPs or SMCs, namely, heat-induced shape memory recovery and retention or self-healing properties, were examined. This work was conducted during the period October 2008-September 2011.

4.2.2.1 Baseline Characterization of High Temperature Thermoplastic SMP Foam Microstructure-Mechanical Stress-Strain Relationships

In this project a commercially available amorphous thermoplastic composition of matter was characterized in order to establish a testing baseline material. The three variants of the same foam, Ultem™ (SABIC Innovative Plastics), a polyetherimide, differed only in average bulk foam volume density and were used for sample preparation as received from the supplier and cut into appropriate test specimens. The specimens were exposed to accelerated conditions of thermal cycling and indirect and direct exposure to short wave ultraviolet radiation in a Xenon-Arc exposure chamber prior to compression testing. Differences in deformation and recovery of the foam specimen microstructure pre- and post-test were recorded by optical microscopy and x-ray micro computed tomography (X-ray CT). Pre-test imaging indicated irregularities in the cell size that was consistent with artifacts of the manufacturing processes since cell size was smaller near the product margins where cell expansion is limited by the mold constraints. When storage moduli (a measure of stiffness) was measured by DMA from samples taken from both the edge and center regions of an Ultem™ composition, it was found within each of the three bulk densities that the room temperature modulus is consistently higher near the margins when compared to the stiffness of the same composition where the average cell size in the center of the product is larger, again attributable to the cell size at location of sample abstraction. DMA data also indicated a consistent T_g which was independent of location of the specimen abstraction or frequency under which the DMA heating rate was operated.

Compression and stress-strain behavior of each of the bulk density foams was evaluated on as-received samples and samples exposed to accelerated conditioning prior to test. The results of the compression tests indicated that the initial elastic yield limit occurred at ~5% strain and was independent of the foam bulk density. Plastic flow initiated at 20-40% strain with little change in stress magnitude between 20-40% strain as cell walls (struts) bend. Beyond 40% strain, struts broke and cells coalesced. As applied strain increased, primary modulus of the foam decreased, attributable to the larger cell sizes and consistent in values with the as-received bulk foam product not along the material margins. Recovery of original sample shape was not achieved upon long strain holds universally across all foam densities. While samples exposed to accelerated radiation and heat suffered no visible damage, they were discolored from off-white to an amber hue. All three specimen densities lost weight, but weight loss magnitude appeared to be inversely proportional to increasing foam density. Overall, though, there was little difference in mechanical performance between as-received and environmentally aged specimens.

Public Domain Publications (Peer Reviewed) and Presentations:

J. T. Fulcher, H. E. Karaca, G. P. Tandon, D. C. Foster, and Y. C. Lu, "Multiscale Characterization of Water-, Oil- and UV-Conditioned Shape-Memory Polymer Under Compression," Proc. SEM 2011 Ann. Conf. on Exper. and Appl. Mech.: Mech. of Time Depend. Mater. and Proc. in Conv. and Multi Funct. Mater., 3 (2011) 97-103.

A. McClung, G. P. Tandon, and J. Baur, "Fatigue Cycling of Shape Memory Polymer Resin," Proc. SEM 2011 Ann. Conf. on Exper. and Appl. Mech.: Mech. of Time Depend. Mater. and Proc. in Conv. and Multi Funct. Mater., 3 (2011) 119-127.

G. P. Tandon, K. Goecke, and R. S. Justice, "Influence of Microstructure and UV Conditioning on the Mechanical Response of Polymeric Foam Under Compressive Loading," Proc. ASME 2011 Conf. Smart Mater., Adapt. Struct. and Intell. Sys. (SMASIS2011), 1 (2011) 103-111. SMASIS2011-5060.

4.2.2.2 Microvascular Self-Healing Composites Mechanical Evaluation

This work is described elsewhere.

4.2.3 Lightweight Flow and Sensing Methods

This subtask objective was to develop novel material systems compositions and characterization approaches for light weight and flow sensing in a reconfigurable, multifunctional structure. When considering the amount of hydraulic lines and wiring bundles there are in a typical commercial aircraft (References 3(a)-(b)), weight considerations in small air vehicles becomes part of the very large problem of balancing performance and mission critical functions against overall systems flyoff weight. This subtask examined methods by which mesoscale reinforcing materials could be prepared and evaluated reliably for some of their most basic mechanical properties for future lightweight systems. For the flow aspect, emphasis of the work was to develop an airflow sensor that could detect wind direction and provide an electrical signal response of some kind for attitude adjustment.

4.2.3.1 Z-Axis CNT Growth Using Chemical Vapor Deposition (CVD) on Conductive Substrates

This project emphasized the efficient and reproducible morphological growth of carbon nanotube bundles known as CNT arrays or CNT forests using CVD. The goal of this project was to directly grow uniform, vertically aligned CNTs, VACNTs, on conductive substrates at the lab scale so that these arrays, rather than single carbon nanotubes, could be evaluated for use as the conductive elements of an airflow sensor. A furnace was constructed and a cleaning methodology was established for preparing planar conductive substrates. The length of the VACNTs could be varied during tube production by varying the depth of the Fe-Al catalyst bed, amount of water vapor present in the furnace, and the composition of the charging gases with the carbon feedstock (References 4-5). The outcome of the experimentation demonstrated that CNTs could be grown on metallic or non-metallic conductive substrates, but the quality of the arrays is not of sufficient high quality for evaluation.

Public Domain Publications (Peer Reviewed) and Presentations: None

4.2.3.2 Z-Axis CNT Growth Using CVD on Nonconductive Substrates and CNT Characterization

Within this project a suite of evaluation techniques was developed or refined that would lead to a means to evaluate deformation of vertically aligned arrays of multiwalled (MW) CNTs (MWCNTs or VACNTs) grown on a non-conductive substrate. The length of the tubes could be varied during tube production by varying the depth of the Fe-Al catalyst bed, amount of water vapor present in the furnace, and the composition of the charging gases with the carbon feedstock (References 4-5). A continuous stiffness measurement (CSM) technique described elsewhere (Reference 6) was employed using an MTS Nanoindenter XP system and a flat punch nanoindentation tip. Amplitude, frequency, displacement slope and load rate were held constant. Arrays of specific tube lengths (i.e., height) were found to exhibit room temperature stress-strain compressive yielding behavior consistent with open cell foams of varying densities at 0.03-0.12 strain. Compressive buckling was also observed in the arrays and documented by scanning electron microscopy (SEM) with structural defects increasing as length (or tube height) increased from substrate attachment. Although an attempt was made to correlate the lateral forces attributable to collapse of the tube into a buckle, its magnitude and contribution to buckle formation was not easily quantifiable except for a very long tube (large aspect ratio) array. Magnitude of the compressive elastic modulus vs. strain was found to be relatively independent of tube lengths and provided more traceability of the observed mechanical properties of MWCNTs to those of open celled foam materials.

In the concurrent work of the project, a means to directly observe the buckling and compressive deformation phenomena of MWCNTs *in-situ* was realized by modifying an SEM chamber with a flat punch nanoindentation tip to apply compressive force to both a vertically aligned 7.5 micron tall, large diameter (i.e., small aspect ratio) MWCNT array with minimal tube entanglement and short tube compressive properties and a 600 micron tall, small diameter (large aspect ratio) MWCNT array with entanglement between neighboring

CNTs whose properties should be closer to foam-like compressive behavior. Buckling behavior was again verified at similar positions on the individual carbon nanotubes as in the previous nanoindentation experiment and the buckling forces observed for the short tubes compared well with theoretical Euler-Bernoulli calculations. The taller MWCNT arrays compared favorably with buckling behavior observed for open celled foams with first buckle formation near the array attach point to the template surface at 2% strain. Recovery height of the large aspect ratio MWCNTs was approximately 70% original height with this packing density used.

Another variation on the refinement of the *in-situ* SEM imaging of real-time VACNT bucking and mechanical behavior enabled strain field mapping using digital imaging correlation (DIC) analytical techniques. What had not been clear to this point was the effect of wide-spread, global, deformation distribution within a VACNT array in an isolated deformation event. Use of DIC typically allowed the mapping of the deformation mechanics in macroscale systems using a dot pattern, impractical of course at the nanoscale. However, the pattern produced on the outer wall when a CNT deforms provided an image contrast at the kink in the tube cell wall as buckling folds formed in the nanotube. The analytical imaging technique was used on square cross-sectional MWCNT arrays to simplify this first attempt of using the technique in-situ to follow room temperature deformation and buckling in both low and high aspect ratio MWCNTs. In both high and low aspect ratio CNTs, the buckling behavior was easily resolved by SEM at 5% local strain.

Finally, all of these techniques to characterize a square cross-sectional MWCNT array were then applied using the *in-situ* SEM compression, DIC of VACNTs and flat punch nanoindentation with the CSM to obtain uniaxial compression and out of plane shear values. Five elastic constants of axial modulus, transverse modulus and out of plane shear modulus, and two measurements of Poisson's ratio, one each in axial and transverse compression, were obtained using the techniques of flat punch nanoindentation with CSM, and *in-situ* SEM compression using DIC analysis respectively. Once these values were identified as representative of a transversely isotropic solid, a Timoshenko beam model was used to predict the VACNT buckling stresses for high aspect ratio square cross-sectional VACNTs. The ultimate outcome of the experiment provided a potential framework in which mechanical or physical properties could be tailored by CNT geometry and density designs.

Public Domain Publications (Peer Reviewed) and Presentations:

M. R. Maschmann, G. J. Ehlert, A. Tawfick, A. J. Hart, and J. W. Baur, "Continuum Analysis of Carbon Nanotube Array Buckling Enabled by Anisotropic Elastic Measurements and Modeling," Carbon 66 (2014) 377-386.

Y. C. Lu, J. Joseph, M. R. Maschmann, L. Dai, and J. Baur, "Rate-Dependent, Large Displacement Deformation of Vertically Aligned Carbon Nanotube Arrays," in Challenges in Mechanics of Time-Dependent Materials and Processes in Conventional and Multifunctional Materials 2 (2013) 101-107 [Springer].

Y. C. Lu, J. Joseph, Q. Zhang, M. R. Maschmann, L. Dai, and J. Baur, "Large Displacement Indentation Testing of Vertically Aligned Carbon Nanotube Arrays," Exp. Mech. 52 (2012) 1551-1554.

M. R. Maschmann, G. J. Ehlert, S. J. Park, D. Mollenhauer, B. Maruyama, A. J. Hart, and J. W. Baur, “Visualizing Strain Evolution and Coordinated Buckling Within CNT Arrays by *In-Situ* Digital Image Correlation,” Adv. Funct. Mater. 22 (2012) 4625-4639.

G. J. Ehlert, M. R. Maschmann, and J. W. Baur, “Electromechanical Behavior of Aligned Carbon Nanotube Arrays For Bio-Inspired Fluid Flow Sensors,” Proc. SPIE 7977, Active and Passive Smart Structures and Integrated Systems, 7977 (2011) 79771C-79771C-15.

M. R. Maschmann, G. J Ehlert, and J. W. Baur, “Piezoresistive Response of Aligned Carbon Nanotube Arrays for Flow Sensing Applications,” Proc. ASME 2011 Conf. Smart Mater., Adapt. Struct. and Intell. Sys. (SMASIS2011), 2 (2011) 673-680. SMASIS2011-5096.

M. R. Maschmann, Q. Zhang, F. Du L. Dai, and J. Baur, “Length Dependent Foam-like Mechanical Response of Axially Indented Vertically Oriented Carbon Nanotube Arrays,” Carbon 49 (2011) 386-397.

M. R. Maschmann, Q. Zhang, R. Wheeler, F. Du, L. Dai, and J. Baur, “*In-situ* SEM Observation of Column-like and Foam-like CNT Array Nanoindentation,” ACS Appl. Mater. Interfaces 3 (2011) 648-653.

Q. Zhang, Y. C. Lu, F. Du, L. Dai, J. Baur, and D. Foster, “Viscoelastic Creep of Vertically Aligned Carbon Nanotubes,” J. Phys. D: Appl. Phys. 43 (2010) 315401-315407.

4.2.3.3 Lightweight and Bio-Inspired Flow Sensing Systems Characterization

As the final project work of this subtask, the electromechanical responses of planar square MWCNT arrays on a non-conductive surface were evaluated. Creep behavior and response time under compressive load for three VACNT arrays were examined. In addition, a prototype demonstration, although not quantified nor idealized in design or procedure, was performed as a concept proof for a single, radially assembled CNT-coated S-2 glass capillary microfiber, evaluated for use as a simulated functional airflow sensor for a flight control structure. Particle image velocimetry was used to map the flow field around a cylindrical capillary in a particulate airflow (Fig. 1; note stagnation point and boundary layer in dark blue.). The flow field data were used to then calculate the force and moment acting on the base of the hair and the results for the calculated drag normal to the hair axis were compared to the electrical response of the hair. Both calculated and experimental drag coefficients compared favorably.

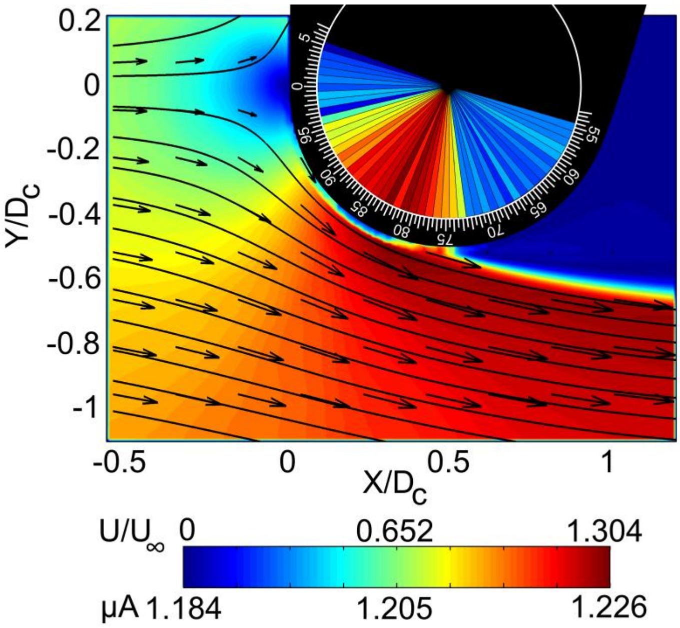

Figure 1. Mean Artificial Hair Sensor Response (Pie Chart Inset) vs. the Flow Field Around the Cylinder [From Ray et al.].

Public Domain Publications (Peer Reviewed) and Presentations:

C. W. Ray, D. M. Phillips, B. J. Hagen, M. R. Maschmann, K. A. Slinker, G. J. Ehlert, B. T. Dickinson, J. W. Baur, and G. W. Reich, "Detection of Flow Separation and Stagnation Points Using Low Inertia, Glass Fiber Artificial Hair Sensors" Bioinspiration and Biomimetics [in preparation].

M. R. Maschmann, G. J. Ehlert, B. T. Dickinson, D. M. Phillips, C. W. Ray, G. W. Reich, and J. W. Baur, "Bio-Inspired Carbon Nanotube Fuzzy Fiber Hair Sensor for Airflow Detection," Adv. Mater. (2014) [accepted for publication].

G. Ehlert, M. Maschmann, D. Phillips, and J. Baur, "Morphology Control in Hierarchical Fibers for Applications in Hair Flow Sensors," Proc. SAMPE 2013 279-293.

M. R. Maschmann, B. Dickinson, G. J. Ehlert, and J. W. Baur, "Force Sensitive Carbon Nanotube Arrays for Biologically-Inspired Airflow Sensing," Smart Mater. Struct. 21 (2012) 094024.

4.2.4 Modeling of Responsive and Configuring Materials

A group of technical effort projects comprise this subtask with the express purpose of modeling or simulating the responsive and configuring materials produced as either SMPs, SMCs or Shape Memory Alloys (SMAs). Effort was assigned to personnel considered experts in specific technical areas of SM material development that could conduct the modeling and simulation activities in an efficient manner with educated, well-designed approaches for experimentation.

4.2.4.1 3-D Analytical Tool Development for SMPs

The tools developed in this project were used to compare 3-D constitutive models for glassy SMPs such as those evaluated in Paragraph 4.2.1.1 and comparing the results of the model with experimental data reported on epoxy-based thermosetting SMPs. Modeling of the thermomechanical processes associated with deformation in SMPs was emphasized and a properly invariant thermodynamic theory capable of predicting the thermal and mechanical behavior of SMP's under a variety of conditions was developed. Solution strategies using these model simulations were then used to benchmark the model and determine the input parameters required for the model. The models for the glassy SMP material both above and below T_g included the notion of "natural configuration" and maximization of stress-strain dissipation. Data fit provided a viscoelastic model with two natural configurations: the behavior of the model is entropic in nature at the higher temperatures above T_g and energetic in nature at the temperature below T_g. Behavior of these predictive models is consistent with what was reported in 4.2.1.1 publications. The modeling code was adapted to ABAQUS (Reference 7) as a subroutine for Finite Element Analysis (FEA).

Public Domain Publications (Peer Reviewed) and Presentations:

K. Yu, A. J. McClung, G. P. Tandon, J. W. Baur and H. J. Qi, "A Thermomechanical Constitutive Model For an Epoxy-Based Shape Memory Polymer and Its Parameter Identifications," J. Mech. of Time-Depend. Mater. 2014 [accepted for publication].

4.2.4.2 Sensory Materials Characterization

The objectives of this modeling project included the modeling of the elastic-plastic deformation and viscoelastic creep of VACNT arrays such as those prepared and evaluated under Paragraph 4.2.3.2. Verification of the models was corroborated with the experimental nanoindentation data acquired in the previous effort. Low speed, large displacement nanoindentation tests were first performed with in-situ indentation inside a SEM. The vertically aligned carbon nanotube arrays exhibited a transient elastic deformation at small displacement and then plastic deformation at large displacement. The critical indentation pressure (P_m) was extrapolated from the indentation stress-displacement curve, which was a measure of the collapsing stress of CNT arrays. The magnitude of P_m at the end of the indenter was found to approximately equal the collapsing stress of the same carbon nanotube array under uniaxial compression, indicating that there was negligible interfacial friction between the nanotubes and the indenter sidewall. FEA simulations using ABAQUS showed that, under the cylindrical flat punch, the nanotube cells collapsed plastically immediately beneath the indenter, a region of the highest stress/strain. The plastic deformation remained relatively unchanged in size at large displacement, corresponding to the plateau region on the load-depth curve. Large displacement indentation tests were also performed at various indenter velocities. The P_m was found to be proportional to the effective strain rate.

Viscoelastic creep in VACNTs was measured from the flat punch nanoindentation experiment. In the test, the indenter was quickly ramped to a control load and then held at the peak for a period of time. Resulting creep response was observed to consist of two stages: (1) a short transient stage and (2) a steady state stage, in which the rate of displacement was constant. The instantaneous control stress and strain rate were monitored during the experiment, and the slope of the natural log of the hardness vs. the natural log of the strain rate yielded the strain rate sensitivity of the nanotube material. The instantaneous modulus of the VACNT array was found to be 58 MPa, although the axial modulus of a single SWNT could be as high as 1 TPa. The strain rate sensitivity depended upon the density of the nanotube arrays. Denser nanotube material had fewer geometric freedoms for tube movement and thus exhibited less creep deformation. It was demonstrated that the strain rate sensitivity of the VACNT array decreased by a factor of 2 simply by doubling the nanotube density.

Public Domain Publications (Peer Reviewed) and Presentations:

Y. C. Lu, J. Joseph, M. R. Maschmann, L. Dai, and J. Baur, "Rate-Dependent, Large Displacement Deformation of Vertically Aligned Carbon Nanotube Arrays," in Challenges in Mechanics of Time-Dependent Materials and Processes in Conventional and Multifunctional Materials 2 (2013) 101-107 [Springer].

Y. C. Lu, J. Joseph, Q. Zhang, M. R. Maschmann, L. Dai, and J. Baur, "Large Displacement Indentation Testing of Vertically Aligned Carbon Nanotube Arrays," Exp. Mech. 52 (2012) 1551-1554.

Q. Zhang, Y. C. Lu, F. Du, L. Dai, J. Baur, and D. Foster, "Viscoelastic Creep of Vertically Aligned Carbon Nanotubes," J. Phys. D: Appl. Phys. 43 (2010) 315401-315407.

4.2.4.3 Fabrication and Modeling of Rubber Muscle Actuators

This project undertook the use of a direct write system to print optimized 3-D polyurethane rubber muscle actuators (RMAs), which were triggered for this experiment by pressurized means and embedded in parallel to rubber elastomeric material skin panels for evaluation. McKibben-like RMA fibers expand and contract like a muscle upon stimulus application and have been traditionally used as natural looking prosthetics for amputees (Reference 8). Assembly and fabrication methodologies were optimized to prepare individual RMAs and test panels with embedded RMAs in order to determine axial contraction and actuator forces under hydraulic or pneumatic pressures of 40-50 psi. FEA models (laminated plate and rod & plate) were developed to simulate contraction and flexure of the individual RMAs and RMAs embedded in the polyurethane matrix. Diameters were optimized for best performance with ½-1 diameter on-center spacings between tube-like RMAs embedded in the polyurethane panels. At these spacings with these materials used, closed valve (CV) to open valve (OV) ratios (a stiffness figure of merit) were consistent for panel performance in force exerted and axial contraction and correlated well with rod & plate FEA models. Laminated plate FEA models were better predictors of the experimental forces output in contraction by the RMAs. A computer aided design program using direct write was also prepared for future fabrication of the RMAs with tougher materials.

Public Domain Publications (Peer Reviewed) and Presentations:

L. D. Peel, L. Muratalla, J. Baur and D. Foster, "The Effect of Scale on Fluid-Filled Composite Actuators," Proc. ASME 2011 Conf. Smart Mater., Adapt. Struct. and Intell. Sys. (SMASIS2011) 2 (2011) 581-590. SMASIS2011-4934.

L. D. Peel, J. Baur, D. Phillips, and A. McClung, "The Effect of Scaling on the Performance of Elastomer Composite Actuators," Proc. SPIE 7644 (2010) 76441 W-1 – 76441 W-12.

4.2.4.4 Modeling of Power Response of SMP/SMA Microactuation

Various approaches to actuation were investigated in the design and initial proof of concept of a viable means by which to quantify the throughput of power to a SMP subcomponent in a RMA design based upon the work of Paragraph 4.2.4.3. Actuation by electrolytic or pneumatic gas generation by biologic or chemical means were explored and FEA models were developed using ABAQUS which predicted the deformation and sealing actions of a slider-valve design (Reference 9) or the tapered biomimetic SMA/SMP pore design upon exposure to the pressurizing force, pressure source indifferent. A horizontal test rig was designed and built for future testing of the optimized biomimetic actuator design embedded in an RMA.

Public Domain Publications (Peer Reviewed) and Presentations:

T. M. Sutter, T. S. Creasy, M. B. Dickerson, and R. S. Justice, "Power Response of a Muscle Actuator Driven by a Regenerative, Enzymatic Pressurization Mechanism," Proc. ASME 2013 Conf. Smart Mater., Adapt. Struct. and Intell. Sys. (SMASIS2013) 2 (2013) V002T06A008. SMASIS2013-3098.

4.2.4.5 Modeling of SMP/Alloy Composites

COMSOL (Reference 15) multi-physics simulations were utilized for agreement with the analytical expressions derived from this work on shape-fixity and interfacial stresses in three operating regimes for SMP/SMA composites. Shape recovery in the operational regimes was provided by the SMAs while shape fixity was provided by the SMPs modeled. It was found that the models produced by COMSOL provided insight into the design of a linear SMP/SMA two-way actuation device.

Public Domain Publications (Peer Reviewed) and Presentations:

J. Park, L. M. Headings, M. J. Dapino, J. W. Baur, and G. P. Tandon, "Analysis of Shape Memory Polymer-Alloy Composites: Modeling and Parametric Studies," Proc. ASME 2012 Conf. Smart Mater., Adapt. Struct. and Intell. Sys. (SMASIS2012) 1 (2012) 227-236. SMASIS2012-8257.

4.3 Task 3.0 Higher Temperature Shape Memory Materials

4.3.1 Thermally Activated SMP Synthesis and Fabrication

In this subtask the projects represented families of thermosetting polymer compositions that exhibit higher glass transition temperatures than the epoxy terminated thermosetting SMP resins of Paragraph 4.2.1.1. This subtask work included not only synthesis and characterization of SMPs but also the mechanical evaluation and durability assessments of shape memory fiber reinforced composite compositions, SMCs, and fabric reinforced SMCs for both lower and higher use temperature resin compositions. The term of this subtask was October 2008 through September 2012.

4.3.1.1 High Temperature Thermosetting BMI-based, Polyaspartimide Resins

In this project a family of five crosslinked polyaspartimide-urea SMPs was prepared that contained tailorable numbers of polymeric pendant crosslink sites, a relatively low T_g range but a large processing window in the rubbery state when compared to SMPs previously prepared. The large processing window allowed model compounds as well as tailored length polymer systems to have SM morphology locked into the SMP without risk of reaching degradation onset temperatures of the polymer pendant crosslinking groups or the linear polymeric backbone. Both the model compounds and the tailored length polymeric systems, consisting of commercially available Matrimid 5292 Part A and Jeffamine D-400 monomers, were then prepared using a modified Michael addition procedure reported elsewhere (Reference 10) and exposed to the mono or diisocyanate crosslinking agent respectively. Crosslink density in the polymer was varied by adjustment of the mole ratio of Jeffamine D-400 to diisocyanate in the polymeric mixture and the weight percentage of polymer in the solvent. Quantitative yields of the polymers were afforded. Upon isolation the family of crosslinked polymers was then individually characterized by elemental analysis, TGA and DMA. Disks of cast polymers, nominally 35 mm dia. X 1 mm thick, were heat treated above T_g near 150°C, deformed into a desired shape, and cooled to demonstrate repeatable shape memory recovery processes in the tough SMP disks. Upon examination of the processing parameters of the SMPs it was found that room temperature viscosity increased with time and temperature and rendered the neat SMP intractable with a very small processing window before complete cure.

Public Domain Publications (Peer Reviewed) and Presentations:

J. A. Shumaker, A. J. W. McClung, and J. W. Baur, "Synthesis of High Temperature Polyaspartimide-Urea Based Shape Memory Polymers," Polymer 53 (2012) 4637-4642.

G. P. Tandon, T. Gibson, J. Shumaker, R. Coomer, R. S. Justice, and J. Baur, "Processing and Characterization of Novel Bismaleimide-Based Shape Memory Polymer Composites," Proc. ASME 2012 Conf. Smart Mater., Adapt. Struct. and Intell. Sys. (SMASIS2012), 1 (2012) 19-25. SMASIS2012-7936.

A. J. W. McClung, J. A. Shumaker, and J. Baur, "Novel Bismaleimide-Based Shape Memory Polymers: Comparison to Commercial Shape Memory Polymers," Proc. ASME 2011 Conf. Smart Mater., Adapt. Struct. and Intell. Sys. (SMASIS2011), 1 (2011) 95-102.

A. J. W. McClung, J. A. Shumaker, J. W. Baur, S. D. Reed, and S. Mathys, "Bismaleimide Based Shape Memory Polymers: Correlation Between Chemical Composition and Mechanical Properties," 52nd AIAA/ASME/ASCE/AHS/ASC Struct., Struct. Dyn. Mater. Conf., 9 pp. AIAA 2011-2012
http://arc.aiaa.org.wrs.idm.oclc.org/doi/pdf/10.2514/6.2011-2112

4.3.1.2 Thermosetting non-BMI SMP Neat Resin Characterization and Assessment

In this project a styrene terminated SMP resin, VF62, was compared to Veriflex-E2-100, an epoxy terminated SMP, for durability and themomechanical performance after environmental exposure. The styrene-based resin (VF62) developed surface microcracks when immersed in oil and became brittle and fractured during handling when exposed to ultraviolet (UV) radiation. On the other hand, the epoxy-based resin (VFE2-100) did not degrade and showed little change in the SM behavior from environmental conditioning and subsequent repeat cycling. Thus, the epoxy-based SMP resin was identified as a candidate resin for morphing applications. The epoxy-based SMP resin had a glassy tensile modulus of 3.1 GPa and developed a recovery stress 0.5-0.6 MPa for a prescribed strain of 75%.

Public Domain Publications (Peer Reviewed) and Presentations:

G. P. Tandon, K. Goecke, K. Cable and J. Baur, "Durability Assessment of Styrene and Epoxy-Based Shape Memory Polymer Resins," J. Intell. Mater. Sys. Struct. 20 (2009) 2127-2143.

4.3.2 Thermally Activated SMCs

In this task a number of activities concerning SMCs were executed in order to extend the thermosetting SMP neat resin technologies previously evaluated into the use of a lightweight load-bearing fabric-reinforced structural composite. The extension into hybrid designs with active cooling channels was explored in the project described in Paragraph 4.3.2.2. Contractual end dates extended the reporting terms until June 2013 for some of the projects of this subtask; hence the delayed reporting in the open literature.

4.3.2.1 Durability Assessment of Fabric Reinforced SMC Laminates

This project is an extension of Paragraph 4.3.1.2 such that the data acquired during the neat resin studies of the two thermosetting polymers was applied to the fabrication, thermomechanical performance, and durability of fabric reinforced epoxy-based SMP composites being considered for morphing applications when separately exposed to moisture, lubrication oil, and UV radiation. This project sought to develop methods for assessing the effects of simulated in-service environments on key performance attributes for fabric-reinforced SM laminates using Veritex^{TM} fabric and VFE2-100^{TM} for the SMC laminates. Test procedures and protocols for evaluating the performance of these SMC materials were developed. The temperature sensed from the black panel temperature probe typically represented the highest temperature that was experienced by the test specimens during accelerated weathering tests, and the chosen value was below the T_g of the material system being studied. In order to develop SMPs for specific morphing applications, quantitative analysis of both shape fixing and shape recovery was a major concern. By performing testing of SMCs in simulated service environments designed to be reflective of anticipated performance requirements, the results of this study established the useful design space for fabric-reinforced SMCs.

Public Domain Publications (Peer Reviewed) and Presentations:

G. P. Tandon, K. Goecke, K. Cable, and J. Baur, "Environmental Durability of Fabric-Reinforced Shape-Memory Polymer Composites," J. Intell. Mater. Sys. Struct., 21 (2010) 1365-1381.

A. J. W. McClung, G. P. Tandon, D. C. Foster, and J. Baur, "Influence of Post-Cure and Repeated Cycling on the Thermomechanical Characterization of Shape Memory Polymers and Composites," Proc. SAMPE 2010, 138-152.

G. P. Tandon, K. Goecke, K. Cable and J. Baur, “Durability Assessment of Fabric-Reinforced Shape Memory Polymer Composites, Proc. ASME Conf. Smart Mater., Adapt. Struct. and Intell. Sys. (SMASIS2009), 1 (2009) 23-32. SMASIS2009-1242.

4.3.2.2 Other Higher Temperature SMCs and Hybrids

In this project two different higher temperature materials systems approaches were examined for achieving a minimal operational use temperature of 250°F (121.11°C) for subsonic aircraft structure. With the use of SMCs in such an application, it was desirable for the composite to reach this minimum thermal threshold without triggering the shape memory mechanism inherent in the composite. Shape recovery and shape fixity were also of interest for the neat resins as well as the composites characterized in this project. Should a higher temperature SMC with all the desirable thermal properties not be achievable by a correct compositional choice, an active heating or cooling approach built directly into the SMC was explored.

Plain weave and unidirectional intermediate modulus 6-ply carbon SMCs were fabricated from a toughened endcapped variant of the BMIs of Paragraph 4.3.1.1 with lower crosslink densities and more polymeric conformational flexibility in the resin matrix. A composite fabrication procedure was developed using an optimized stoichiometric resin composition of 70% flexible backbone moiety to 30% siloxane endcap and a target of 30-35% fiber volume in the final consolidated composite coupons. Room temperature and elevated temperature data was collected under flexural load using a three-point bend test for both neat resin and composite flat panel coupons. Good shape fixity and shape recovery was realized in the final SMC of >84% and >94% respectively over 5 heating cycles to 150°C.

Public Domain Publications (Peer Reviewed) and Presentations:

G. P. Tandon, T. Gibson, R. Coomer, and J. Baur, “Thermo-Mechanical Performance and Fatigue Cycling of Novel Bismaleimide-Based Shape Memory Polymer Resin and Composites,” Proc. ICCM 19, (2013).
http://confsys.encs.concordia.ca/ICCM19/AllPapers/FinalVersion/TAN81395.pdf

Quasi-isotropic intermediate modulus unidirectional carbon fiber reinforced epoxy composite laminates were embedded with micro channels that were formed in the prepreg prior to traditional autoclave cure with stainless steel tube inserts or upon ply layup on a removable mandrel. The channels were therefore either lined with stainless tubes or unlined in the final cured laminate. Fracture toughness was examined as a function of channel diameter and orientation to adjacent fiber plies by cantilever beam testing. Surface temperature profiles were observed during internal fluid flow and natural convection by thermography. A two-dimensional analytical model was then developed using a Fourier transform series to explain thermal transport within the test specimens and a framework was established using an active heating/cooling approach to high temperature thermosetting SMCs. The analytical model compared favorably with the experimental thermography tests.

Public Domain Publications (Peer Reviewed) and Presentations:

K. Yu, D. M. Phillips, J. W. Baur and H. J. Qi, “Analysis of Shape Memory Polymer Composites with Embedded Microvascular System for Fast Thermal Response,” J. Compos. Mater. (2014) [accepted for publication].

D. M. Phillips, R. M. Pierce, and J. W. Baur, "Mechanical and Thermal Analysis of Microvascular Networks in Structural Composite Panels," Composites A 42 (2011) 1609-1619.

4.4 Task 4.0 Support of AFOSR Hybrid Material Flight Structures Multi-University Research Initiative (MURI)

4.4.1 Fabrication of Composite Flat Panels

As a participant and vested partner in the MURI technical outcomes for Texas A&M University, both neat resin and composite test panels were fabricated containing commercially available Matrimid 5292 bismaleimide as the polymer resin matrix with T300 plain weave carbon fabric for the composite laminates. Additional composite panels consisting of the MURI start date was CY 2009 with a five-year term (Reference 11).

4.4.1.1 Fabrication of Bismaleimide (BMI) Resin Panels

Flat panels of neat Matrimid BMI thermosetting resin were prepared with and without 8 wt% Polyethersulfone thermoplastic resin toughener. A resin film infusion process with vacuum bagging was employed in order to prepare consolidated flat panels. The autoclave cure cycle was optimized and a total of 39 panels of various sizes and shapes of test specimens with a range of thicknesses between 1-12 mm were fabricated, characterized and delivered to the lead university for test. C-scan and SEM were used to detect the absence of voids in the consolidated samples or uniform dispersion of the toughener in the resin matrix.

Public Domain Publications (Peer Reviewed) and Presentations: None

4.4.1.2 Fabrication of BMI/Graphite Composite Panels with Resin Tougheners and Multifunctional Nanofibers

Composite flat panel laminates of plain weave T-300 graphite woven cloth with Matrimid BMI thermosetting resin were prepared with and without 8 wt% Polyethersulfone thermoplastic resin toughener and were resin infused into $[0/90]_x$ layups. A modified bagging and cure cycle that accounts for the presence of the fiber reinforcement in the composite was employed to prepare laminates with a range of thicknesses between 1-12 mm. C-scan and SEM were used to detect the absence of voids in the consolidated coupons or the uniform dispersion of the toughener in the resin matrix. A total of 31 out of 35 flat panels of various sizes and thicknesses, with the exception of four 12 mm thick panel coupons, were delivered to the lead university.

Public Domain Publications (Peer Reviewed) and Presentations: None

4.5 Task 5.0 Nanomodified Carbon and Fiber Characterization For DoD Database

Work effort was requested in the past and in current work efforts of the Materials and Manufacturing Directorate, AFRL, to provide the DoD with an independently assessed materials database for the characterization of COTS, modified COTS and novel materials compositions and processing of carbon fiber and to conduct the work as an independent testing agency. PE 6.2 funding was supplied by the Government agency to AFRL/RX for the work efforts. AFRL/RXCC possesses a unique capability if needed to heat treat carbon fiber compositions onsite with both carbonization and graphitization furnaces. The work described in the subtasks of Task 5.0 was conducted from October 2009 through September 2011.

4.5.1 Commercial Fiber Modifications

4.5.1.1 Modified High Modulus C-Fiber Characterization

Nine 50 filament each of carbon fiber tow samples were received from the Government agency and characterized as-received. Half were modified high modulus PAN-based fibers from commercial sources and the remaining were experimental carbon fibers. On the whole, the commercial fiber tows were on the order of 5 micron diameter and the experimental fiber tows were between 7-8.4 micron diameter when measured by light microscopy and FAVIMAT single filament test techniques. With the assumption of a fiber density of 1.8 g/cm, a typical value for PAN-based carbon fiber, room temperature tensile strengths and moduli were determined. With three of the four larger diameter experimental fibers it was found that the tensile moduli were an order of magnitude lower than the high modulus commercial fibers, more reflective of values seen in IM-7 intermediate modulus carbon fiber. However, the smallest 7 micron experimental fiber possessed tensile properties in modulus and strength closer to the high modulus commercial fiber tows, typically in the order of 160-180 N/tex.

Public Domain Publications (Peer Reviewed) and Presentations: None

4.5.1.2 Boron Carbide Fiber

Mechanical testing was not possible on these fibers due to the lengths and small numbers of experimental fibers supplied, well below the minimum test samples of 20 for relevancy and test validity. Due to the fragility of the fibers it was also not possible to extract some of them from their adhesive paper mountings without breakage. For Raman spectroscopy the seven experimental fibers were compared to highly oriented graphitic pitch based P-100 and strong but less oriented PAN-based AS-4 carbon fibers. The fibers showed little orientation when compared to P-100 standard and more closely resembled a less oriented AS-4 standard with broader and lower peak wavenumbers. Due to the angular orientation of the graphene sheet planes in the experimental boron carbide fibers relative to the fiber axis, the mechanical, electrical and thermal properties of the fibers were less than expected.

Public Domain Publications (Peer Reviewed) and Presentations: None

4.5.2 High Temperature Nanotube Yarns and Composite Characterization

Nanotube yarn doping with solvents or acids (Reference 12) or possibly by annealing the yarns under tension (Reference 13) has been reported to improve the electrical conductivity of the tubes to values near that of copper. In a simple attempt to verify the basic yarn mechanical properties, two samples of five filament average densified nanotube yarns were exposed to a spray of polar solvent or polar solvent/water absorbing polymer. When compared to the control, the doped yarns doubled in density and shrunk about 21% of their original diameter. A 20% drop in tensile strength and a 50% drop in strain to failure were observed in the solvent/polymer exposed yarn and a 57% drop in strength and 68% drop in strain to failure observed in the solvent only doped yarn. Since little was known about the method of fabrication of the samples, a more comprehensive test with more samples and fiber diameters and fiber twists under varied fabrication conditions was planned for future work.

Thermal conductivity measurements were performed on pitched based carbon fibers with axial graphene sheet orientation similarly described in Paragraph 4.5.1.2. The technique of laser flash analysis was used to estimate the thermal conductivity by adjusting the laser flash data for highly oriented graphitic fibers. FEA was used to simulate the heat flow patterns that might possibly occur in a uniaxial polymer matrix composite. Thermal conductivity was accurately simulated in composites with high fiber volume fractions of 60% even with low thermally conductive fibers. For high conductivity fibers with low fiber volume fractions of 20% it was found that the FEA was not as accurate since the heat flow paths of the highly oriented pitch-based conductive fibers may deviate transversely rather than follow a 2-D pathway.

Public Domain Publications (Peer Reviewed) and Presentations:

R. M. Alway-Cooper, M. Theodore, D. P. Anderson, and A. A. Ogale, "Transient Heat Flow in Unidirectional Fiber-Polymer Composites During Laser Flash Analysis: Experimental Measurements and Finite Element Modeling," J. Compos. Mater. 47 (2013) 2399-2411.

4.6 Task 6.0 Polymeric Nanocomposites

In this task work effort emphasized the construction of nanoscale biomaterials interfaces for uses in bioactuation and diagnostics or even as a battery storage material. For higher use temperature applications, the use of carbonaceous precursors of structural carbon, namely graphitic or graphene nanomaterials, appear attractive. The goal of the work herein was to develop processing methods and characterization of 2-D graphene oxides upon which inorganic compositions or biomaterials could be self-assembled. The subtask and project work was initiated in October 2008 and concluded in March 2012.

4.6.1 Organic and Inorganic Polymer Nanocomposite Alloys

Graphene Oxide (GO) was prepared from a modified procedure previously reported (Reference 14) and processed into a film from a series of acidic and highly dilute aqueous solution washes. Aminosilane and polydimethylsiloxane moieties respectively occupied the interstitial spaces in the GO sheet conformations by soaking and heating the GO films in an aqueous solution of excess reagent with extended gentle heating, subsequent reduction with hydrazine vapor and hydrolysis with copious amounts of water. An exfoliated colloid of organic or inorganic/GO nanocomposite resulted when the dried films were suspended in water and separated through ultrasonic treatment. After characterization by FTIR and Raman spectroscopy and microscopy (SEM), the nanocomposites were evaluated for their thermal analytical properties using TGA. Electrical conductivity was measured using four probe method before and after reduction with hydrazine vapor. Exfoliated sheets were measured at 1 nm thickness in comparison to pristine graphene at 0.34 nm, attributable to the presence of the covalent sp^3 carbon bonds formed above and below the plane of the 2-D graphene sheet with the aminosiloxane or polydimethylsiloxane moieties. Conductivity was improved in the aminosiloxane/GO nanocomposite after the reduction with hydrazine as measured by four probe. In contrast, the polydimethylsiloxane groups were sterically so large, the conductivity by four probe remained in the insulating range both before and after hydrazine reduction. An insulating layer of polydimethylsiloxane was found on the surface of the GO sheet by X-ray photoelectron spectroscopy (XPS).

Public Domain Publications (Peer Reviewed) and Presentations: None

4.6.1.1 DNA/Graphene Oxide (GO) Synthesis, Processing and Characterization

GO was prepared in like manner to the procedure described in Paragraph 4.6.1 and processed into a film from a highly dilute aqueous solution. Deoxyribonucleic acids (DNA) occupied the interstitial spaces in the GO sheet conformations and exfoliated dried films were produced from sonicated colloids. Full characterization was performed using the techniques described in Paragraph 4.6.1. XPS spectra, corroborated by SEM imaging, showed that the DNA was uniformly dispersed on the surface. Further morphological investigations by SEM and Raman before and after reduction clearly showed the aggregation of DNA domains in the interstitial spaces in thin film cross-section and reduction of the GO sheets by increased intensity of the D and G bands in the Raman spectra respectively. Improved contiguity of the film properties as measured by four probe increased conductivity values from insulating to conductive after hydrazine reduction of GO sheets, thus also indicating complete reduction by the hydrazine of any surface oxygen residues still present.

Public Domain Publications (Peer Reviewed) and Presentations:

Z. Bai, "Morphological and Physical Properties of DNA/Graphene Layered Bio-Nanocomposites," Polym. Prepr. 52(2) (2011) 278-79.

4.6.1.2 Gold/Polymer Nanocomposite Synthesis

Functionalized gold nanoparticles were prepared in commercially available poly(4-vinylpyridine) or polyvinylpyrrolidone using aqueous media and processed to produce 20 wt% loaded aggregated nanoparticles. Effective size of the aggregates was measured using dynamic light scattering which confirmed the aggregation of 5-6 nanoparticles per cluster. SEM verified the size of the highly organized densely packed nanoclusters after deposition on a glass slide at 39.7 nm for the gold/poly(4-vinylpyridine) nanocomposites. Strong peaks in the optical absorption spectra indicated absorption near 520 nm for the plasmon excitation resonance.

Public Domain Publications (Peer Reviewed) and Presentations: None

4.6.2 Polymeric Nanocomposite Battery Materials

4.6.2.1 GO/Polyethylene Oxide (PEO) Synthesis and Processing

This project investigated improved synthesis and the processing approaches to develop more dimensionally and thermally stable battery materials for solid state lithium ion batteries. GO was prepared in like manner to the procedure described in Paragraph 4.6.1 with the addition of an aqueous solution of PEO. Cast films of the GO/PEO nanocomposite in 75-100 micron thicknesses were prepared from 5-15 wt% loadings and the films reduced in hydrazine vapor. Increased loadings of the GO showed the formation of a uniform ordered network, but the processing was not optimized nor characterized any further as in Paragraph 4.6.1.1-4.6.1.2.

Public Domain Publications (Peer Reviewed) and Presentations: None

4.7 Task 7.0 Ongoing Work from AAM for Completion

This catch-all task tracked the completion of customer funded 6.2 PE work that was required to honor program commitments. The mélange of efforts included foam-filled composite sandwich structures evaluation, research quantity level characterization of novel "fuzzy" carbon fibers, and a durability assessment of a COTS thermosetting resin. What is not included in this task description is an effort in materials integration into a subtask in morphing materials. The term of this task work was October 2008 through September 2011.

4.7.1 Mechanical Testing of Thermosetting Foams for Airfield Matting

In this subtask, two candidate polymer matrix composite (PMC) sandwich structures were evaluated in flat panel for compressive and flexural mechanical properties. One candidate structure consisted of carbon fiber reinforced epoxy composite facesheet filled with syntactic foam between the integrated composite struts, perpendicular to the facesheets, while the alternate candidate system was comprised of quasi-isotropic carbon fiber reinforced epoxy composite facesheets and a foam filler with the entire sandwich stitched through the thickness of the panel. Two additional candidate monoliths of unfilled, hexagonal aluminum honeycomb core with differences in cross-sectional cell size and height were evaluated in compression only. Using self-leveling compressive platens, replicate 4 inch square PMC candidates and 2 inch diameter metallic samples were tested for room temperature compressive properties. In addition, the PMC samples were cut for test in four-point bend with flex load, both perpendicular and parallel to the critical extrusion or span directions. Both metallic honeycomb candidates compressively buckled in the gage sections of the specimens under compressive loading, as expected, but the larger unit cell length (i.e., shorter in height) was incrementally better in compressive strength by 170 psi over the narrower, more dense, and taller honeycomb specimens. For the PMC candidates, room temperature compressive strength values for the integrated strut candidates showed improved strength values over the stitched PMC with mode of failure of the stitched coupons by buckling of the resin tubes and shear fracture along the foam margins in the samples but were still lower by as much as an order of magnitude than the metallic honeycomb. The mechanical response in flex load of the PMC candidates is non-linear due to damage initiation early in the loading of the specimens at the samples' edges, so test to failure was not assessed. When a reinforcing span is parallel to the extrusion direction in an integrated strut PMC composite coupon for four point bend, a larger load is carried by the PMC (31%) and it is as much as three times as strong as the stitched PMC sample in either direction (i.e., parallel or perpendicular to the extrusion direction) of the quasi-isotropic composite sandwich.

Public Domain Publications (Peer Reviewed) and Presentations: None

4.7.2 C-Fiber Synthesis and Characterization

This work is described elsewhere.

Public Domain Publications (Peer Reviewed) and Presentations: None

4.7.3 Morphing Materials

This work is described elsewhere.

Public Domain Publications (Peer Reviewed) and Presentations: None

4.7.4 Miscellaneous Durability Subtasks

This subtask work concluded a carry-over effort from the prior branch in-house program in which a full characterization of PMR-15 polyimide resin was conducted using a sharp-tipped Berkovich diamond tipped nanoindenter equipped with a hot-stage heating system to evaluate the creep rate and creep effect in this COTS high use temperature thermosetting resin. The indentation experiments utilized the “hold-at-the-peak” method at various indenter holding times and unloading rates. The normalized creep rate, a measure of creep effect, decreased with increasing indenter holding time and/or unloading rate. Procedures used to minimize the creep effect were investigated at both ambient and 200°C so that the correct contact depth (together with modulus and hardness) could be determined from the nanoindentation load-depth curve. The temperature dependent mechanical properties of PMR-15 were consistent with those obtained from macroscopic tests. Analytical procedures were modified to take into account the holding time and unloading rate so that the correct contact depth, along with elastic modulus and hardness, could be calculated. The effective holding time was determined for PMR-15 at both ambient and elevated temperatures. Statistical analysis revealed that the variations in nanoindentation measurements performed at elevated temperatures were at a minimum, thus indicating that the current high temperature nanoindentation technique was reliable for quantitative characterizations of mechanical properties of polymers/composites at elevated temperatures.

Public Domain Publications (Peer Reviewed) and Presentations:

Y. C. Lu, D. C. Jones, G. P. Tandon, S. Putthanarat, and G. A. Schoeppner, “High Temperature Nanoindentation of PMR-15 Polyimide,” Exp. Mech. 50 (2010) 491-499.

4.8 Task 8.0 Graded Polymeric-Preceramic Hybrid Materials

The technical problem of this task to resolve, which was carried over from the HEE Program, was to address the immiscibility between an organic polymeric and a preceramic polymeric material. Reactive diluents are usually incorporated into thermosetting resin systems to provide either chemical compatibility for processing or to impart mechanical toughness to a final resin composition. The diluents typically provide additional spacing between polymer chains, imparting additional spatial volume and degrees of freedom to polymer chains, or the backbone may contain pendant side groups that are somewhat more chemically compatible with the immiscible portion of the mixture by providing bonding sites or, in contrast, physical entanglement. After years of unsuccessful approaches to solving the miscibility problem with the dissimilar polymer and preceramic processing approaches (Paragraph 4.8.2), a unique chemical resolution to the technical problem was attempted with the approach described in Paragraph 4.8.1. The technical work of this entire task was conducted from October 2008-June 2012.

4.8.1 Synthesis of BMI/Preceramic Polymer Compatibilizers

The work of this subtask was to mitigate or eliminate the morphological issue of phase separation in a graded hybrid preceramic–thermoset transition layer consisting of Starfire RD-730-Matrimid blend, via the incorporation of suitably designed polymeric compatibilizers, and subsequent cure. The structural motif of the compatibilizers synthesized via a hydrosilylation–deprotection sequence was primarily based on a polymer repeat unit with a nonpolar segment consisting of a carbosilane unit and a polar segment with a bisphenol A-type moiety. Besides the homopolymer, two block copolymer systems with varying proportions of a nonpolar block containing a carbosilane with an aliphatic hydrocarbon link and a more polar block containing a bisphenol A unit linked to a carbosilane were also synthesized and characterized. The effectiveness of the compatibilizers, incorporated in small quantities for alleviating phase separation in the blends, was assessed by the Starfire domain size and distribution observed in the SEM of cured specimens. The block copolymer, designed to have an equal number of the nonpolar and polar block repeat units, was found to be reasonably effective in mitigating phase separation. However, the incorporation of the homopolymer that was most polar due to the highest phenolic content in its structure resulted in a dramatic reduction of the Starfire domain size, down to <5mm in diameter in the cured Starfire–Matrimid blend. The presence of this compatibilizer was also found to result in the uniform distribution of Starfire domains in the samples examined as well.

Based on the post-processing observations above, the compatibilizers were identified as follows in terms of decreasing effectiveness to minimize phase separation of the Starfire domains as well as promote homogeneity in the cured resin plaques, in accordance with decreasing polarity from the homopolymer compatibilizer 3 to block copolymer compatibilizer 2: compatibilizer 3 (5 wt%) > compatibilizer 3 (1 wt%) > compatibilizer 1 (5 wt%) > control > compatibilizer 2 (5 wt%).

Public Domain Publications (Peer Reviewed) and Presentations:

AFRL-RX-WP-TP-2014-0023, “Bismaleimide/Preceramic Polymer Blends for Hybrid Materials Transition Regions: Part 2. Incorporating Compatibilizers [Postprint],” January 2014. DTIC Accession # ADA592889.

B. R. McKellar, N. Venkat, S. Safriet, J. M. Brown, M. R. Unroe, V. Bechel and E. Fossum, “Bismaleimide/Preceramic Polymer Blends for Hybrid Materials Transition Regions: Part 2. Incorporating Compatibilizers,” High Performance Polymers 25 (2013) 399-415.

4.8.2 Processing of BMI/Preceramic Polymer Blends

In this project, initial steps were taken in the study of processing mixtures of a carbonaceous polymer matrix resin and a preceramic polymer to produce a hybrid material that contained a region of gradual transformation from a polymer to a ceramic. It was thought to be the first step toward the eventual development of a hybrid that was graded from a PMC to a CMC. Blends of RD-750 preceramic polymer, which converts to silicon carbide upon pyrolization, and Matrimid 5292 A/B polymer, a BMI, were conducted as a function of cure cycle. The cure cycles were chosen to vary resin viscosity at specific times during processing in order to affect the amount of phase separation between the two resins. These results were then used to conclude the effect of processing parameters on resin miscibility and the likelihood of producing a hybrid with mechanical and thermal properties that fall between those of the two individual polymer constituents. High RD-730 loadings were realized without phase inversion, the T_g of the blended material was shown to be significantly influenced by post-cure conditions, and a spatial gradient in RD-730 was noted.

Blends of the RD-730 and Matrimid A/B were successfully fabricated by hot-melt mixing followed by casting and curing. The effects of composition and cure cycle variations on the morphology and thermal properties of the blends were investigated using SEM, DSC, TGA, and DMA. In summary, a wide range of experiments showed that altering the processing cycle did not lead to a significantly increased miscibility. This was unfortunate, since an increased miscibility would indicate that the RD-730 and Matrimid A/B were chemically reacting or mixing sufficiently to potentially result in a new material with a stiffness, temperature capability, and CTE in the property space between that of RD-730 and Matrimid A/B. As a result, this project work served as a motivation to move to more radical approaches in the fabrication of a BMI/preceramic polymer hybrid. In the work described in Para 4.8.1, the success achieved in using chemical compatibilizers added as a third constituent which take advantage of polarization differences of the two base constituents for improved miscibility was described. Thus this work was used for baseline materials development in the previous subtask.

Public Domain Publications (Peer Reviewed) and Presentations:

AFRL-RX-WP-TP-2014-0022, "Bismaleimide/Preceramic Polymer Blends for Hybrid Materials Transition Regions: Part 1. Processing and Characterization [Postprint]," January 2014. DTIC Accession # ADA592890.

V. T. Bechel, S. Safriet, J. M. Brown and M. R. Unroe, "Bismaleimide/Preceramic Polymer Blends for Hybrid Materials Transition Regions: Part 1. Processing and Characterization," High Performance Polymers 25 (2013) 363–376.

4.9 Task 9.0 Hybrid Material Processing and Fabrication

In this task, also originating from the Hybrid Materials for Extreme Environments Initiative Program, subtask work was conducted to develop approaches to the fabrication and processing of dissimilar materials monoliths into an integrated hybrid structure using traditional and nontraditional processing and fabrication approaches. Graded attachment and link hardware were explored with limited success and reported elsewhere as was the use of increased surface adhesion in metal to PMC monoliths, but an approach to examine the graded concept from a metallic to a PMC hybrid joint was feasible with newly emerging processing technologies.

4.9.1 Traditional Processing

This subtask work is reported elsewhere.

4.9.2 New Combinatorial Processing Approaches

4.9.2.1 Processing and Fabrication of Hybrid Metal to Composite Joint

In this subtask, the approach of a metallic to carbon fiber reinforced PMC hybrid joint was explored in order to develop a novel hybrid material fastening proof of concept. Processing by an additive manufacturing approach, namely laser engineering net shape (LENS), was explored as a possible processing method to lay down graded metallic to graded PMC hybrid layers without the use of adhesive bonds between two materials monoliths. Titanium foils were used as substrates in order to deposit a titanium powder grade by LENS into intermediate modulus, T-300 carbon fiber fabric (NAHF-X^{TM}). Once the desired metallic-carbon fiber preform was constructed at 0.12 inch thickness, a PMC was built up using fully imidized powder of MVK-14 resin (Renegade) that was consolidated and infused into the fabric voids using traditional consolidation processing techniques for compression molding. Some voids were noted in the central region of the hybrid by SEM, but the processing parameters for this proof were not optimized at the conclusion of the Composite and Hybrid Materials ERA. Other fabrication approaches such as selective metal laser sintering, direct metal laser sintering, e-beam melting or even thermal spray techniques are possibilities to explore for future fabrication work on PMC-metallic hybrids as well as production of consolidated, flat panel hybrid materials test coupons larger than 6 in X 6 in.

Public Domain Publications (Peer Reviewed) and Presentations:

T. Whitney, T. Gibson, K. Lafdi, V. Bechel, and B. Welk, “Hybrid Metal-to-Composite Joint Fabricated Through an Additive Manufacturing Process,” Proc. ASME Int. Mech. Eng. Cong. and Exp. 3A, B, C (2012) 929-932. IMECE2012-89540.

4.10 Program Management

To execute the technical portion of the Program Management task, weekly technical meetings were conducted to communicate current technical effort with the entire AFRL/RXCC community. Occasionally guest speakers were invited from outside the immediate community to enlighten the participants and to give presentations on current state of the art materials and processing topics. Presentations in the public domain were given by participants in the program technical work as it progressed or concluded, and these presentations are enumerated in the national conference proceedings cited in this document. Responsibility for review of manuscripts, presentations and technical documents prior to release was shared by the technical leads, program managers, and AFRL/RX management. Once work was completed, manuscripts were submitted to peer reviewed journals for publication where appropriate. Both presentations and peer reviewed publications are listed in the citations at the end of Section 4.0 paragraphs of this document. Financial tracking was accomplished by the respective program managers with AFRL/RX management and business operations staff for the 6.2 PE funded efforts in order to maintain up-to-date budgeting and funds management, funds earnings and expenditure information in all pertinent cost categories. Program management accountability was captured in internal documents such as laboratory, business and program management reviews and this final report for the program.

5.0 CONCLUSIONS AND RECOMMENDATIONS

Since this is a programmatic roll-up of the entire four-year in-house program effort, there are no conclusions or recommendations to provide. From a historic aspect, several of the technologies reported in this document either provide insight for possible directions for current or future technical work within the Structural Materials Division of AFRL/RX, and to the knowledge of the author, the only work disclosed in this report that continued beyond the conclusion of the Composite and Hybrid Materials ERA in the Table 1 WBS was the work of Para 4.9.2, and that continued work was easily disengaged from the work documented here. Otherwise, all tasks, subtasks, and projects listed in Table 1 are concluded and reported elsewhere or described the public domain publications listed in Section 4.0 of this document.

REFERENCES

1. M. Unroe, Internal AFRL/RX Program Documentation (2008).

2. M. Unroe, Internal AFRL/RX Program Documentation (2011).

3(a). N.d. Photograph. n.p. Web. 27 Mar 2014.
http://www.aircanada.com/en/about/fleet/historical/b747-400.html

3(b). N.d. Photograph. n.p. Web. 27 Mar 2014.
http://wiki.answers.com/Q/How_many_miles_of_wiring_in_a_Boeing_747

4. S. Chakrabarti, K. Gong, and L. Dai, "Structural Evaluation Along the Nanotube Length for Super-Long Vertically Aligned Double-Walled Carbon Nanotube Arrays," J. Phys. Chem. C 112 (2008) 8136-8139.

5. K. Hata, D. Futaba, K. Mizuno, T. Namai, M. Yumura, and S. IIjima, "Water-assisted Highly Efficient Synthesis of Impurity-free Single-Walled Carbon Nanotubes," Science 306 (2004) 1362-1364.

6. S. Pathak, G. Cambaz, S. Kalidindi, G. Swadener, Y. Gogotsi, "Viscoelasticity and High Buckling Stress of Dense Carbon Nanotube Brushes," Carbon 47 (2009) 1969-1976.

7. ABAQUS 2010 ABAQUS Users' Manual (Pawtucket, RI: Hibbit, Karlson and Sorenson Inc.)

8. H. F. Schulte, Jr., "The Characteristics of the McKibben Artificial Muscle," The Application of External Power in Prosthetics and Orthotics, National Academy Science-National Resource Council, Washington, D. C., 1961.

9. M. Kohl, Shape Memory Microactuators. Microtechnology and MEMS, ed. H. Baltes 2004, Heidelberg: Springer-Verlag. 247.

10. Z. Shen, J. Schlup and L. Fan, "Synthesis and Characterization of Leather Impregnated With Bismaleimide (BMI) – Jeffamine Resins," J. Appl. Poly. Sci. 69 (1998) 1019-1027.

11. N.d. Photograph n.p. Web. 28 Mar 2014.
http://muri18.tamu.edu/Assets/Papers/Overview_Lagoudas.pdf

12. T. McDonald, J. Elliott, and J. Kitaygorsky, "Carbon Nanotube Additives for Electromagnetic Compatibility of Composites, 42nd ISTC (2010).

13. J. S. Bulmer, L. M. Christie, D. P. Anderson, G. Kozlowski, J. M. Petry, B. T. Quinton, C. Jayasinghe, G. Li, J. H. Lee, H. Wan, B. Ruter-Schoppman, K. Yost, and P. N. Barnes, "Bulk Carbon Nanotube Yarn Conductivity and Strength Enhancement Through High Temperature Annealing," Carbon 2010 (2010) 628-629.

14. W. Hummers and R. Offeman, JACS 80 (1958) 1339.

15. COMSOL, N.d. Photograph n.p. Web 9 Apr 2014 http://www.comsol.com/products

LIST OF SYMBOLS, ABBREVIATIONS AND ACRONYMS

2-D – Two dimensional

3-D – Three dimensional

AAM – Adaptive, Active, and Multifunctional Composite and Hybrid Materials Program

ABAQUS – A commercially available finite element analytical modeling tool

AFRL/RX – Air Force Research Laboratory, Materials and Manufacturing Directorate

AFRL/RXBC – Composite and Hybrid Materials Branch, Nonmetallic Materials Division, AFRL/RX

AFRL/RXCC – Composites Branch, Structural Materials Division, AFRL/RX

BMI – Bismaleimide, a high temperature thermosetting polymer composition

CAD – Computer Aided Design

CMC – Ceramic Matrix Composite

CNT – Carbon nanotube

COMSOL – A commercially available multi-physics modeling program

COTS – Commercial-off-the-Shelf

CSM – Continuous Stiffness Measurement

CVD – Chemical Vapor Deposition

CY – Calendar Year

DIC – Digital Image Correlation

DNA – Deoxyribonucleic Acid

DSC – Differential Scanning Calorimetry

DMA – Dynamic Mechanical Analysis

ERA – Exploratory Research Area

Fe-Al – Iron-Aluminum

FEA – Finite Element Analysis, a computerized 2-D or 3-D analytical tool using a mesh and node system to model and simulate structural loads on complex structures

GFY – Government Fiscal Year

GO – Graphene Oxide

HEE – Hybrid Materials for Extreme Environments Initiative Program

LCP – Liquid Crystalline Polymer

LENS – Laser Engineering Net Shape

MURI – Multi-University Research Initiative

MWCNT – Multi-Walled Carbon Nanotube

P_m – Critical Indentation Pressure

PE – Program Element

PMC – Polymer Matrix Composite

RMA – Rubber Muscle Actuator

SEM – Scanning Electron Microscopy

SM – Shape Memory

SMA – Shape Memory Alloy, consisting of more than one materials composition with shape memory characteristics, such a metal and an organic polymer

SMC – Shape Memory Composite, a reinforcing component and a matrix of materials dissimilarity

SMP – Shape Memory Polymer

SWNT – Single Walled Nanotube

T_g – Glass transition temperature; the temperature at which a polymeric material changes from a glassy state to a rubbery state

TGA – Thermogravimetric Analysis

UV – Ultraviolet

VACNT – Vertically Aligned Carbon Nanotube

X-ray CT – X-ray micro Computed Tomography

XPS – X-ray Photoelectron Spectroscopy